NICOLAUS COPERNICUS UNIVERSITY IN TORUŃ

Bulletin of Geography. Physical Geography Series, No. 31 (2026): 49–65
http://doi.org/10.12775/bgeo-2026-0010

# Comparative use of remote sensing and in-situ data for chlorophyll-a estimation in urban lakes: a case study of Chitgar Lake, Tehran, Iran

**Javad Bayat[1*], Maryam Rouhi Kerigh[2], Afsaneh Shahbazi[3], Mehdi Karami[4], HamidReza Heidari[5]**

[1,4]Shahid Beheshti University, Environmental Sciences Research Institute, Tehran, Iran

[2]Isfahan University of Technology, Department of Environment, Natural Resources Faculty, Isfahan, Iran

[3]Shahid Beheshti University, Department of Environmental Technologies, Environmental Sciences Research Institute, Tehran, Iran

[5]Gorgan University of Agricultural Sciences and Natural Resources, Department of Environmental Science, Gorgan, Iran

*Correspondence e-mail: J_bayat@sbu.ac.ir

[a]https://orcid.org/0000-0002-2544-6805

**Abstract.** Chlorophyll-a (Chl-a) is a key indicator of phytoplankton biomass and freshwater quality and is strongly influenced by nutrient availability, seasonal variability and climatic conditions. This study investigates the spatiotemporal dynamics of Chl-a in Chitgar Lake, an artificial urban lake in Tehran, Iran, by integrating long-term in-situ observations (2013–2025) with satellite-derived estimates from Sentinel-2 and Landsat-8. Seasonal analysis revealed that Chl-a concentrations were highest during summer (mean: 2.93 mg/m$^3$), peaking in August (3.53 mg/m$^3$), coinciding with elevated water temperatures (up to 30.8°C) and reduced dissolved oxygen (mean: 8.35 mg/L), indicative of eutrophic conditions. In contrast, winter and spring exhibited lower Chl-a levels associated with cooler temperatures and more stable oxygen conditions. The mean total phosphorus concentration (0.03 mg/L) suggests phosphorus limitation, consistent with international eutrophication thresholds. Four satellite-based algorithms – Two-Band Ratio, Normalized Difference Chlorophyll Index (NDCI), Three-Band Difference Algorithm (3BDA), and Maximum Chlorophyll Index (MCI) – were evaluated using S2 and L8 imagery. Sentinel-2 consistently outperformed Landsat-8, with NDCI achieving RMSE of 1.23 mg/m$^3$, MAE of 0.93 mg/m$^3$, and $R^2$ of 0.68. Seasonal validation identified fall as the most reliable period for Chl-a estimation (RMSE: 0.88–1.03 mg/m$^3$), while winter showed the lowest errors but limited explanatory power ($R^2$: 0.23–0.28). Landsat-8 yielded acceptable performance, particularly in spring ($R^2$: 0.64–0.84), despite its coarser spatial resolution. Spatial Chl-a maps derived from NDCI revealed consistent distribution patterns between satellites and strong agreement with in-situ measurements. However, Sentinel-2's finer spatial resolution (10–20 m) enabled improved detection of small-scale variability. Overall, the results highlight the value of Sentinel-2 red-edge bands for Chl-a retrieval in optically complex inland waters, while confirming the continued importance of Landsat-8 for long-term trend analysis. The findings emphasize the need for local calibration and support integrated satellite – in-situ monitoring frameworks for improved eutrophication management in urban lakes.

**Key words:** Chlorophyll-a, Remote Sensing, Eutrophication, Chitgar Lake, Iran

© Author(s) 2026. This work is distributed under the Creative Commons Attribution 4.0 License (http://creativecommons.org/licenses/by-nc-nd/4.0/).

## Introduction

Algae and phytoplankton are essential components of aquatic ecosystems, serving as primary producers and contributing significantly to biogeochemical cycles. Their growth is closely linked to nutrient availability, particularly nitrogen and phosphorus, with Chlorophyll-*a* (Chl-*a*) being a widely used indicator of phytoplankton biomass and productivity. Eutrophication refers to a situation in aquatic environments characterized by elevated nutrient levels, particularly nitrogen and phosphorus. This excess of nutrients leads to the proliferation of algae, ultimately diminishing the water quality within these ecosystems (Bali and Gueddari 2019; Sonarghare et al. 2020). Water quality is a crucial environmental aspect because it impacts both people and their economic activities. Recent studies have demonstrated how eutrophication can lead to harmful algal blooms, which adversely affect water quality and biodiversity (Paerl and Paul 2020; Dembowska et al. 2022). One of the major water quality issues worldwide is the occurrence of harmful algal blooms, which produce toxins and worsen both aquatic ecosystems and human public health (Hallegraeff et al. 2021). Furthermore, monitoring Chl-*a* concentrations provide valuable insights into the ecological health of lakes and can help in managing eutrophication (Baker et al. 2021; Zhang et al. 2023). These findings illustrate the critical interplay between nutrient dynamics, algal growth and the overall health of freshwater ecosystems. In Chitgar Lake, elevated levels of phosphorus and nitrogen compounds have been linked to increased algal growth and subsequent declines in water quality (Bayat et al. 2021). Algal blooms not only reduce light penetration but also deplete dissolved oxygen levels during decomposition phases, leading to hypoxic conditions detrimental to aquatic organisms. The consequences of eutrophication extend beyond ecological impacts; they also pose economic challenges related to tourism and recreation. As algal blooms become more frequent or severe due to nutrient loading from urban runoff or agricultural practices, recreational opportunities diminish along with aesthetic values associated with clean water bodies.

Remote sensing has emerged as a vital tool in environmental monitoring, providing unprecedented capabilities for assessing and managing aquatic ecosystems. The application of remote sensing technologies allows for the collection of data over large spatial scales and at regular intervals, making it possible to track changes in water quality, vegetation cover and land use. For over 25 years, satellite remote sensing technology has allowed for comprehensive and timely observation of water quality (Mishra et al. 2019). This approach has become increasingly important in the context of freshwater lakes, where parameters such as Chl-*a* serve as critical indicators of ecological health. Eutrophication in lakes can be evaluated using sensor products due to the spectrally active nature of Chl-*a* (Buma and Lee 2020). Although many studies have focused on estimating Chl-*a* concentrations in oceans and estuaries through remote sensing, inland water bodies have been comparatively neglected (Topp et al. 2020). Significant effort has been devoted to estimating Chl-*a* concentrations in lakes; however, the optical complexity and limited availability of *in-situ* data pose challenges in accurately assessing Chl-*a* levels in these water bodies (Buma and Lee 2020).

Remote sensing also offers a cost-effective means to monitor water quality parameters across extensive geographical areas without the need for exhaustive field sampling. By employing satellite imagery, researchers can detect changes in Chl-*a* concentrations and assess turbidity levels more efficiently than traditional methods (Kumar et al. 2017). The integration of multisensor remote sensing data with *in-situ* observations can substantially improve water quality assessment and management strategies, providing essential support for environmental monitoring programs. For instance, studies have demonstrated that satellite-derived estimates of Chl-*a* correlate well with ground-based measurements, allowing for more comprehensive monitoring efforts (Gholizadeh et al. 2016). Furthermore, remote sensing enables the identification of spatial patterns in water quality that may not be apparent through localized sampling efforts (Park et al. 2024). Recent advancements in satellite technology have revolutionized the monitoring of water quality parameters over large spatial scales. Sentinel-2 (S2) and landsat-8 (L8) satellites provide high-resolution imagery that can be utilized to derive estimates of Chl-*a* concentrations, turbidity levels, and total suspended solids through various algorithms (Kumar et al. 2017). These remote sensing methods enhance our understanding of lake dynamics and facilitate timely interventions to mitigate water quality issues. For example, Sentinel-2 offers multispectral imagery with a spatial resolution of up to 10 meters, enabling detailed assessments of water

bodies (Drusch et al. 2012). The satellite's spectral bands are particularly useful for detecting chlorophyll concentrations due to their sensitivity to specific wavelengths associated with chlorophyll absorption and reflectance. Similarly, Landsat 8 provides a longer historical dataset that is invaluable for trend analysis over time. Despite the advantages offered by remote sensing technologies, several challenges remain in accurately estimating water quality parameters using satellite imagery. Factors such as atmospheric interference, cloud cover and varying water depths can complicate the interpretation of satellite data (Zhang et al. 2018).

This study focuses on the development of predictive equations for estimating Chl-*a* concentration in Chitgar Lake, an urban water body. By integrating observed *in-situ* data with satellite imagery from L8 and S2, our primary objective is to establish robust models that correlate water quality parameters with spectral reflectance values. This approach uniquely leverages the high spatial and temporal resolution of these satellite platforms to provide a detailed assessment of water quality. Our original contribution lies in the application and validation of these specific satellite algorithms within the unique context of an urban lake. We aim to not only monitor water quality dynamics over time but also to deepen the understanding of how the lake's status is influenced by urbanization and local conditions – such as shifts in lake boundaries, water turbidity, and the effectiveness of management strategies like protection programs for preventing algal blooms. This emphasis on an urban lake environment and the specific impacts of its surrounding conditions distinguishes our approach. The resulting predictive equations will serve as valuable tools for efficiently assessing the ecological health of Chitgar Lake, thereby guiding targeted management practices, particularly those aimed at mitigating issues common in lakes near urban centers. Ultimately, this research contributes to the broader fields of environmental monitoring and sustainable management of freshwater resources by providing a comprehensive framework for water quality assessment that integrates advanced remote sensing techniques with crucial *in-situ* measurements.

## Materials and methods

### Study area

Chitgar Lake with geographical coverage ranging from latitude 35.739° N to 35.750° N and longitude from 51.206° E to 51.222° E (Fig. 1), located in the north-west of Tehran city, is an artificial lake designed to enhance recreation and aesthetics. It spans about 1.31 km$^2$ with an average depth of 3.5 meters and a maximum depth of 9.5 meters. The lake features

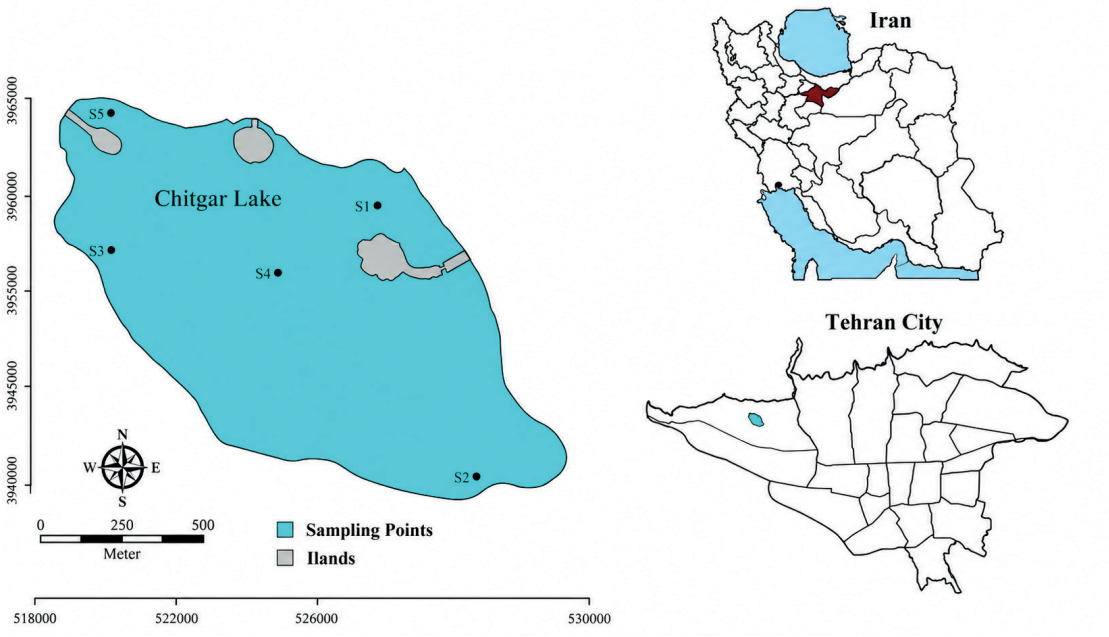


Fig. 1. Chitgar Lake in Tehran city, with monitoring stations

geomembrane and geotextile lining to prevent water loss, holding a total volume of ~6,900,000 m³ at an elevation of 1,267.5 meters above sea level; volume can drop to ~5,200,000 m³ during dry seasons. All information regarding this lake is provided by Bayat et al. (2021).

## Data collection and variables

Monitoring of chlorophyll-*a* and turbidity at five designated stations within Chitgar Lake commenced in April 2013 and will continue based on its designed monitoring plan. Chl-*a* is an indicator of the productivity of water and is measured in lake water to assess concentrations of algae and phytoplankton present. Turbidity indicates the clarity of water and is determined by the amount of light scattered by particles present in the water. The sampling frequency was established at biweekly intervals from 2013 to 2023, transitioning to weekly and daily sampling in 2024 and 2025. Samples were collected using Vandorn sampler and pre-washed glass bottles, transferred to lab immediately and analyzed using the standard method for the extraction of water and wastewater (Method 10200 H). Additionally, for the analysis of frequent samples, the bbe AlgaeOnlineAnalyser II was utilized to measure Chl-*a* concentrations directly from the samples.

## Methodology

### Remote sensing approach

For current research, we utilized Google Earth Engine as the primary tool for processing satellite imagery from SENTINEL-2 and LANDSAT-8 to estimate Chl-*a* concentrations and turbidity levels. Google Earth Engine offers a powerful cloud-based platform that enables efficient handling of large datasets, making it exceptionally well-suited for environmental monitoring applications.

Image Acquisition: In this study, images from Landsat 8 and Sentinel-2 satellites were employed to estimate Chl-*a* concentrations and turbidity, both of which are essential for assessing water quality and the health of aquatic ecosystems. The analysis utilized Landsat 8 images from Collection 2 Tier 1 Level 2, which offer high-quality surface reflectance data that minimizes atmospheric effects and enhances the accuracy of parameter estimations. For Sentinel-2 imagery, a distinction was made between two processing levels based on the acquisition dates (Table 2): images captured prior to the introduction of Level-2A (L2A) were processed using Level-1C (L1C) data, which provide top-of-*a*tmosphere reflectance values. Following the implementation of L2A, imagery with atmospheric corrections was utilized, resulting in a more accurate depiction of surface reflectance. This meticulous selection of satellite imagery facilitates a more precise estimation of Chl-*a* concentrations and turbidity, effectively leveraging the strengths of both satellite systems to enhance the reliability of the findings. The Multispectral Imager (MSI) on the Sentinel-2 mission and the Operational Land Imager (OLI) on Landsat-8 are especially noteworthy for generating reliable water quality assessments due to their strong calibration and robust performance (Buma and Lee 2020). To minimize the impact of cloud cover on Chl-*a* estimations, a cloud masking function was applied to both L8 and S2 imagery. Cloud cover can significantly distort the spectral reflectance, leading to inaccurate assessments (Frouin et al. 2019). The function leverages the quality assessment bands provided with the satellite data to identify and remove cloud-contaminated pixels, ensuring that only relatively cloud-free pixels are used in the subsequent Chl-*a* estimation process. In total, 94 images from L8 were selected (resulting in 473 data across 5 stations) and 79 images from S2 (yielding 395 data across 5 stations) for analysis. Figure 2 illustrates the flowchart of the process cycle for this work.

Indices: In this study, we employed three distinct indices to estimate Chl-*a* concentrations in lake water using satellite imagery: the 2-Band model, the Normalized Difference Chlorophyll Index (NDCI) and the Green Normalized Difference Vegetation Index (GNDVI). Table 1 provides an overview of the remote sensing algorithms applied in this study to Landsat 8 and Sentinel-2 data for Chl-*a* estimation, including formulas and some references.

### Statistical methods

To rigorously assess the performance of Chl-*a* estimation models derived from remote sensing data, a suite of statistical metrics is essential. These metrics provide insights into the accuracy, precision and potential biases inherent in model predictions. Four key metrics, namely Mean Absolute Error (MAE), Root

Table 1. Satellite-based indices for estimating Chl-a concentrations in aquatic systems

| Satellite | Algorithm | Formula | Description | Some References | Band's Range | | | |
|---|---|---|---|---|---|---|---|---|
| Landsat 8 | 2BAND | B5 / B4 | Leverages the reflectance difference between near-infrared and red bands to estimate Chl-*a* concentration. | Gitelson et al. (2008) | Band | Band Name | Central Wavelength (nm) | Spatial Resolution (m) |
| | NDCI | (B4−B3) / (B4+B3) | Normalizes the difference between green and red bands, reducing atmospheric effects and variations in total suspended solids, making it sensitive to Chl-*a* variations in eutrophic waters. | Mishra and Mishra (2012) | B2 | Blue | 482 | 30 |
| | | | | | B3 | Green | 561 | 30 |
| | | | | | B4 | Red | 655 | 30 |
| | GNDVI | (B3−B2) / (B3+B2) | Sensitive to chlorophyll content in vegetation/phytoplankton. Landsat-8 and Sentinel-2 use the same band for this. | Gitelson, Kaufman and Merzlyak (1996) | B5 | Near Infra-Red | 865 | 30 |
| Sentinel-2 | GNDVI | (B3−B2) / (B3+B2) | Sensitive to chlorophyll content in vegetation/phytoplankton. Landsat-8 and Sentinel-2 use the same band for this. | Gitelson, Kaufman and Merzlyak (1996) | Band | Band Name | Central Wavelength (nm) | Spatial Resolution (m) |
| | 2BAND | B5 / B4 | Similarly to Landsat 8, uses the ratio of near-infrared to red bands to estimate Chl-*a* concentration. | Gitelson et al. (2008) | B2 | Blue | 490 | 10 |
| | | | | | B3 | Green | 560 | 10 |
| | | | | | B4 | Red | 665 | 10 |
| | NDCI | (B5−B4) / (B5+B4) | The standard NDCI formula is based on green and red bands. | Mishra and Mishra (2012) | B5 | Vegetation Red Edge | 705 | 20 |

Mean Squared Error (RMSE), Power of test, and R squared, are commonly employed to evaluate model effectiveness.

MAE (Seegers et al. 2018) quantifies the average magnitude of errors in a set of predictions, irrespective of their direction (over- or underestimation). It is calculated as:

$$MAE = \frac{1}{n}\sum_{i=1}^{n} |yi - \hat{y}i|$$

where n is the number of data points, $y_i$ represents the observed values, and $\hat{y}_i$ denotes the predicted values. MAE provides a straightforward measure of prediction accuracy, with lower values indicating better model performance.

RMSE (He et al. 2021) measures the average magnitude of the error and gives more weight to larger errors due to the squaring process, making it particularly sensitive to outliers. The formula is:

$$RMSE = \sqrt{\frac{1}{n}\sum_{i=1}^{n}(yi - \hat{y}i)^2}$$

As a result of its sensitivity to outliers, RMSE is useful in identifying models that may have occasional large deviations from observed values.

Power refers to the probability that a test will correctly reject the null hypothesis when the alternative hypothesis is true, thereby detecting a true effect if one exists (Verzani, 2004). It is influenced by factors such as sample size, effect size, and significance level. A higher power reduces the risk of Type II errors (failing to detect a true effect) and ensures the reliability of results.

$Power = 1 - \beta$

where $\beta$ is the probability of a Type II error.

All statistical analyses were conducted using R software (R Core Team 2023), a widely recognized platform for data manipulation, modeling and visualization. Key metrics such as RMSE, MAE, $R^2$ and power calculations were implemented using base R functions.

## Results and discussion

The analysis of Chitgar Lake's water quality parameters (Table 3) reveals seasonal interactions between Chl-*a*, dissolved oxygen (DO), oxygen saturation,

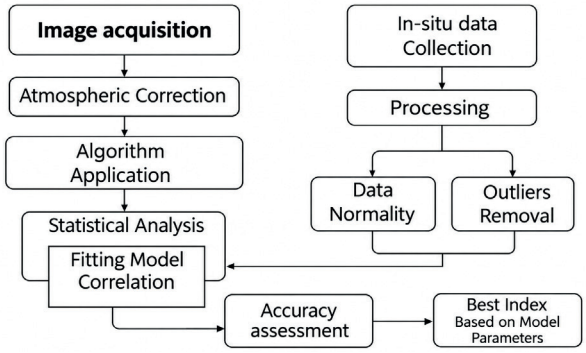


Fig. 2. Work flowchart illustrating the processing cycle

Although this TP value appears low, it falls within the critical threshold range (0.02–0.03 mg/L) identified by Carlson (1977) and Nürnberg (2009) as sufficient to trigger substantial increases in Chl-*a*. Conversely, winter (mean Chl-*a*: 1.39 mg/m³) and spring (1.42 mg/m³) exhibit lower Chl-*a* levels, aligning with cooler conditions and higher DO stability. Monthly trends highlight July–August as critical periods, with Station 4 (mean: 2.05 mg/m³) and Station 3 (2.03 mg/m³) showing elevated Chl-*a*, likely due to localized nutrient inputs. Comparative studies have shown that total phosphorus concentrations significantly influence Chl-*a* levels in various inland waters. For instance, studies by Carlson (1977) and Nürnberg

Table 2. Summary of satellite imagery used for Chl-a estimation in Chitgar Lake

| Parameter | Landsat-8 OLI | Sentinel-2 MSI |
|---|---|---|
| Number of images | 94 | 79 |
| Acquisition period | 12 Jun 2013 – 12 Feb 2025 | 12 Aug 2015 – 12 Mar 2025 |
| Processing level | Collection 2 Tier 1 Level-2 (L2) | L1C (2015–17) and L2A (2017–25) |
| Spatial resolution | 30 m (all bands) | 10 m (B2,B3,B4,B8); 20 m (B5,B6,B7) |
| Bands used for Chl-*a* | B2 (Blue), B3 (Green), B4 (Red), B5 (NIR) | B2 (Blue), B3 (Green), B4 (Red), B5 (Red-edge 1), B6 (Red-edge 2), B7 (Red-edge 3), B8 (NIR) |
| Atmospheric correction | LaSRC (provided with L2 product) | L1C: Sen2Cor applied manually; L2A: built-in Sen2Cor |
| Cloud masking | QA_PIXEL band (pixel_qa) | QA60 band |
| Total data points (5 stations) | 470 (94 × 5) | 395 (79 × 5) |

temperature, and total phosphorus (TP). The mean Chl-*a* concentration was 3.16 mg/m³. Elevated Chl-*a* levels during summer (mean: 2.93 mg/m³), peaking in August (3.53 mg/m³), correlate with warmer temperatures (up to 30.80 °C) and nutrient availability, while reduced DO (mean: 8.35 mg/L) and oxygen saturation (103.42%) during these months suggest algal respiration and decomposition depleting oxygen reserves – a hallmark of eutrophic systems. This inverse relationship between Chl-*a* and DO during warm months is consistent with algal respiration and post-bloom decomposition processes, which deplete oxygen reserves in nutrient-enriched systems (Sonarghare et al. 2020; Dembowska et al. 2022). The mean TP concentration was 0.03 mg/L, indicating low phosphorus levels, which is typical in some inland water bodies but may also suggest a potential limitation on algal growth depending on nutrient dynamics.

(2009) affirm that phosphorus limits algal blooms, identifying thresholds around 0.02 to 0.03 mg/L that can trigger substantial increases in Chl-*a* concentrations. Moreover, research conducted by Brehob et al. (2024) in North American lakes indicated that lakes with TP concentrations exceeding 0.05 mg/L frequently exhibit algal blooms, whereas lower levels are typically associated with clearer waters and lower Chl-*a*. Thus, phosphorus limitation in Chitgar Lake may be intermittent rather than absolute, with localized internal loading or pulsed external inputs (particularly at Stations 3 and 4) driving summer blooms. The lower Chl-*a* levels in winter and spring reflect temperature-limited growth and higher DO stability, aligning with typical seasonal phytoplankton dynamics in temperate inland waters (Paerl and Paul 2020).


Citation: Bulletin of Geography. Physical Geography Series 2026, 31, http://doi.org/10.12775/bgeo-2026-0010

Table 3. Summary statistics for water quality variables in Chitgar Lake (June 2013–March 2025)

| Variables | Unit | Mean | Median | Min | Max |
|---|---|---|---|---|---|
| Chl-*a* | $mg/m^3$ | 3.16 | 2.58 | 0.06 | 15.30 |
| DO | mg/L | 8.34 | 8.05 | 3.97 | 12.56 |
| DO Saturation | % | 103.02 | 102.15 | 59.55 | 133.50 |
| Temperature | °C | 19.27 | 21.28 | 3.80 | 30.45 |
| TP | mg/L | 0.03 | 0.03 | 0.01 | 0.20 |
| **Chl-*a* concentration trend** | | | | | |
| Stations | 1 | 2.70 | 1.92 | 0.01 | 8.60 |
| | 2 | 2.14 | 1.44 | 0.10 | 13.19 |
| | **3** | **2.51** | **1.95** | **0.04** | **13.40** |
| | **4** | **2.70** | **2.00** | **0.04** | **17.66** |
| | 5 | 3.03 | 2.15 | 0.01 | 9.74 |
| Monthly | Jan | 1.32 | 1.36 | 0.04 | 3.28 |
| | Feb | 1.18 | 1.03 | 0.01 | 4.73 |
| | Mar | 1.88 | 1.94 | 0.20 | 4.00 |
| | Apr | 2.44 | 2.53 | 0.10 | 4.74 |
| | May | 1.93 | 1.48 | 0.04 | 6.60 |
| | June | 2.68 | 1.68 | 0.04 | 8.46 |
| | **July** | **4.54** | **4.00** | **1.07** | **17.66** |
| | Aug | 4.13 | 3.82 | 1.00 | 9.74 |
| | **Sep** | **4.50** | **5.10** | **0.52** | **13.19** |
| | Oct | 4.09 | 4.70 | 0.26 | 8.73 |
| | Nov | 1.49 | 1.44 | 0.17 | 4.20 |
| | Dec | 1.27 | 1.20 | 0.10 | 3.50 |
| Seasonal | **Autumn** | **3.34** | **2.32** | **0.17** | **13.19** |
| | Spring | 2.12 | 2.00 | 0.04 | 6.60 |
| | **Summer** | **3.80** | **3.40** | **0.04** | **17.66** |
| | Winter | 1.27 | 1.20 | 0.01 | 4.73 |

Regarding the reliability of input data and limitations related to data quality, the accuracy of Chl-*a* estimation models depends critically on the quality of satellite data and *in-situ* measurements. In this study, *in-situ* Chl-*a* and TP data were collected from Chitgar Lake between 2013 and April 2025 through standardized sampling protocols. However, potential limitations include infrequent ground sampling during certain seasons (e.g., winter ice-covered periods) and spatial mismatches between point-based field measurements and pixel-based satellite reflectance values (Gholizadeh et al. 2016). Such mismatches can introduce uncertainties, particularly in heterogeneous water bodies like Chitgar Lake, where nearshore areas may exhibit different optical properties compared to deeper zones (Topp et al. 2020). Furthermore, atmospheric correction remains a significant source of uncertainty, especially for Landsat-8 OLI, which lacks the red-edge bands present in Sentinel-2 MSI. The standard atmospheric correction algorithms (e.g., Sen2Cor for S2 and LaSRC for L8) are optimized for ocean or clear inland waters and may perform suboptimally in turbid or eutrophic conditions (Frouin et al. 2019). In the present study, no regional tuning of atmospheric correction was applied, which may have contributed to the higher RMSE values observed in

Landsat-8 models (2.23–2.28 mg/m³) compared to Sentinel-2 (1.23–1.37 mg/m³). Users should therefore exercise caution when applying these models without site-specific recalibration.

Table 4 summarizes the statistical results of Chl-*a* estimation algorithms derived from S2 and L8 satellite data. The validation metrics, including RMSE, MAE, $R^2$, adjusted $R^2$ and statistical power, provide valuable insights into the accuracy and reliability of the developed models for estimating Chl-*a* concentrations. These metrics not only reflect model performance but also highlight the influence of satellite specifications and algorithm design on predictive accuracy. The S2 satellite demonstrated varying performance in Chl-*a* estimation across its indices, with the 2BAND, NDCI and GNDVI algorithms showing notable results. The 2BAND index achieved an RMSE of 1.37 mg/m³ and an MAE of 1.05 mg/m³, indicating relatively low error in predictions compared to observed values. The $R^2$ and adjusted $R^2$ values of 0.64 and 0.62 suggest moderate explanatory power, with the model effectively capturing a portion of the variations in Chl-*a* concentrations. This $R^2$ value is somewhat lower than the $R^2$=0.89 reported by Mishra and Mishra (2012) in their initial development of the NDCI for turbid productive waters, but it aligns with results from Pirasteh et al. (2020), where $R^2$ values ranged from 0.65 to 0.78. The equation for this algorithm reflects a cubic relationship between reflectance values and Chl-*a* concentrations, consistent with established optical properties of chlorophyll pigments in water. Additionally, the statistical power of 1.00 indicates a near-certain likelihood that the model avoids Type II errors, affirming its reliability for practical applications. The NDCI algorithm presented an RMSE of 1.23 mg/m³ and an MAE of 0.93 mg/m³. Its $R^2$ value of 0.68 and adjusted $R^2$ value of 0.67 indicate moderate to good explanatory power for estimating Chl-*a* concentrations. These results are comparable to those of Ansper and Alikas (2019), who found an $R^2$ of 0.68 evaluating Sentinel-2's performance in a small lake. However, Chen et al. (2020) reported a higher correlation coefficient of 0.85 using an optimal two-band ratio model for urban lakes. The equation for this algorithm shows a cubic relationship. The GNDVI algorithm also performed well, with an RMSE of 1.26 mg/m³ and an MAE of 0.95 mg/m³, achieving $R^2$ and adjusted $R^2$ values of 0.66 and 0.65, respectively, indicating good explanatory power for Chl-*a* estimation in this study area. The equation for this algorithm also reflects a cubic relationship. These findings align with previous research demonstrating that red-edge bands significantly improve Chl-*a* estimation accuracy in turbid waters – a feature absent from L8 sensors but present in S2 MSI data – highlighting Sentinel-2's potential suitability for inland water monitoring applications compared to Landsat-8 sensors in this study area configuration.

The accuracy of Chl-*a* estimates in inland waters depends on multiple factors that influence water reflectance, including Chl-*a* concentration, the presence of other optically active components, and the complexity of the remote sensing algorithms. When analyzing seasonal performance for S2, winter exhibited the lowest error metrics across all indices, with RMSE values ranging from 1.81 to 1.88 mg/m³ and MAE values between 1.46 and 1.55 mg/m³. However, winter models demonstrated limited explanatory power with $R^2$ values ranging from 0.23 to 0.28, suggesting that while predictions were precise, they captured minimal variability in the winter Chl-*a* distribution, potentially due to lower overall Chl-*a* concentrations. Spring models achieved variable error metrics, with RMSE values ranging from 1.04 to 1.11 mg/m³ and showed the poorest explanatory capability overall, with $R^2$ values ranging from 0.23 to 0.32. Summer predictions exhibited moderate error among all seasons, with RMSE values ranging from 1.01 to 1.05 mg/m³, though with lower explanatory power ($R^2$: 0.21 to 0.26) compared to other seasons, potentially indicating variability in Chl-*a* distribution due to thermal stratification and algal blooms. Fall emerged as the optimal season for S2 Chl-*a* estimation, achieving the best balance between accuracy and explanatory power across all indices, with $R^2$ values ranging from 0.25 to 0.27, and RMSE values ranging from 0.88 to 1.03 mg/m³, while all indices maintained strong statistical power of 0.97 to 0.98. These seasonal variations align with Beck et al. (2016), who concluded that algorithm performance varies based on lake characteristics (turbidity, trophic state), and they underscore the necessity of season-specific calibration.

The L8 satellite demonstrated varying levels of performance across its indices, with the 2BAND, NDCI and GNDVI algorithms yielding different results. The 2BAND algorithm achieved an RMSE of 2.26 mg/m³ and an MAE of 1.65 mg/m³, with a strong $R^2$ value of 0.69, indicating that this algorithm can reliably estimate Chl-*a* concentrations under certain conditions. The equation for this algorithm reflects a cubic relationship. The NDCI index achieved an RMSE of 2.23 mg/m³ and

Table 4. Summary of statistical results for Chl-a estimation algorithms in lake water using S2 and L8 data

| Image Source | Data Subset | Indices | RMSE | MAE | $R^2$ | Adj* $R^2$ | Power | Equation |
|---|---|---|---|---|---|---|---|---|
| Sentinel-2 | Total dataset | 2BAND | 1.37 | 1.05 | 0.64 | 0.62 | 1.00 | Chl-*a* = 0.44 – 1.94 * (X) – 11.8 * ($X^2$) + 112.71 * ($X^3$) |
| | | **NDCI** | **1.23** | **0.93** | **0.68** | **0.67** | **1.00** | **Chl-*a* = 6.65 + 0.11 * (X) – 0.18 * ($X^2$)** |
| | | GNDVI | 1.26 | 0.95 | 0.66 | 0.65 | 1.00 | Chl-*a* = 0.5 – 0.44 * (X) – 0.57 * ($X^2$) - 0.22 * ($X^3$) |
| | Spring | 2BAND | 1.11 | 0.84 | 0.32 | 0.24 | 1.00 | - |
| | | NDCI | 1.04 | 0.79 | 0.23 | 0.18 | 0.95 | - |
| | | GNDVI | 1.04 | 0.80 | 0.23 | 0.17 | 0.95 | - |
| | Summer | 2BAND | 1.01 | 0.77 | 0.26 | 0.21 | 0.98 | - |
| | | NDCI | 1.03 | 0.77 | 0.25 | 0.20 | 0.97 | - |
| | | GNDVI | 1.05 | 0.81 | 0.21 | 0.16 | 0.92 | - |
| | Fall | 2BAND | 1.03 | 0.80 | 0.25 | 0.20 | 0.97 | - |
| | | NDCI | 0.88 | 0.71 | 0.27 | 0.21 | 0.98 | - |
| | | GNDVI | 1.01 | 0.79 | 0.27 | 0.21 | 0.98 | - |
| | Winter | 2BAND | 1.88 | 1.55 | 0.23 | 0.18 | 0.97 | - |
| | | NDCI | 1.81 | 1.46 | 0.28 | 0.24 | 1.00 | - |
| | | GNDVI | 1.83 | 1.49 | 0.25 | 0.21 | 0.99 | - |
| Landsat-8 | Whole dataset | 2BAND | 2.26 | 1.65 | 0.69 | 0.68 | 1 | Chl-*a* = -2612.41 + 8230.62 * (X) – 8636.21 * ($X^2$) + 3018.51 * ($X^3$) |
| | | **NDCI** | **2.23** | **1.63** | **0.70** | **0.69** | **1** | **Chl-*a* = 2.34 + 47.16 * (X) – 223 * ($X^2$) + 341.76 * ($X^3$)** |
| | | GNDVI | 2.28 | 1.69 | 0.65 | 0.64 | 1 | Chl-*a* = –8.68 + 435.93 * (X) – 7152.73 * ($X^2$) + 39351.05 * ($X^3$) |
| | Spring | 2BAND | 1.51 | 1.20 | 0.79 | 0.62 | 0.88 | - |
| | | NDCI | 1.64 | 1.36 | 0.64 | 0.35 | 0.56 | - |
| | | GNDVI | 1.44 | 1.19 | 0.84 | 0.72 | 0.96 | - |
| | Summer | 2BAND | 2.46 | 1.85 | 0.67 | 0.65 | 1 | - |
| | | NDCI | 2.45 | 1.83 | 0.67 | 0.66 | 1 | - |
| | | GNDVI | 2.42 | 1.82 | 0.66 | 0.65 | 1 | - |
| | Fall | 2BAND | 2.42 | 1.81 | 0.66 | 0.65 | 1 | - |
| | | NDCI | 2.45 | 1.83 | 0.67 | 0.66 | 1 | - |
| | | GNDVI | 2.42 | 1.81 | 0.66 | 0.65 | 1 | - |
| | Winter | 2BAND | 2.46 | 1.88 | 0.62 | 0.61 | 1 | - |
| | | NDCI | 2.46 | 1.88 | 0.62 | 0.61 | 1 | - |
| | | GNDVI | 2.48 | 1.89 | 0.63 | 0.62 | 1 | - |

an MAE of 1.63 mg/m³, with a strong $R^2$ value of 0.70. The GNDVI index achieved an RMSE of 2.28 mg/m³ and an MAE of 1.69 mg/m³, with a strong $R^2$ value of 0.65. Regarding seasonal variations in L8 predictions, winter demonstrated the lowest error metrics across all indices, with RMSE values ranging from 2.46 to 2.48 mg/m³ and MAE values ranging from 1.88 to 1.89 mg/m³, and the GNDVI algorithm achieving the highest explanatory power ($R^2$: 0.62 to 0.63) during this season. Spring models showed relatively high explanatory capability, with $R^2$ values ranging from 0.64 to 0.84 and RMSE values from 1.44 to 1.64 mg/m³. Summer exhibited moderate error values (RMSE: 2.42 to 2.46 mg/m³) across all indices with $R^2$ values around 0.66 to 0.67, showing stable seasonal predictive performance, with slightly improved explanatory power compared to winter. Fall predictions showed similar performance across all Landsat-8 indices, with RMSE values ranging from 2.42 to 2.45 mg/m³ and explanatory capability of $R^2$=0.66–0.67, consistent with summer trends. These seasonal trends align with findings from Augusto-Silva et al. (2014), who emphasized the need for local calibration and validation due to varying algorithm performance under different conditions.

The comparison between S2 and L8 satellites reveals that S2 generally outperformed L8 across comparable indices in terms of RMSE and MAE values, although L8 sometimes achieved higher $R^2$ values. This is likely attributable to S2's higher spatial resolution (10–20 m vs. L8's 30 m), inclusion of red-edge bands optimized for Chl-*a* detection, and shorter revisit time (5 days vs. L8's 16 days). For instance, while both satellites' NDCI algorithms showed differences in explanatory power (S2 $R^2$=0.68 vs. L8 $R^2$=0.70 for the total dataset), S2's algorithms achieved lower RMSE values overall. This is supported by Toth et al. (2021), who noted that Chl-*a* estimation depends on the algorithm used and water conditions. This finding is primarily attributable to four sensor-specific advantages of Sentinel-2. First, its higher spatial resolution (10–20 m vs. Landsat-8's 30 m) reduces mixed-pixel effects in optically complex waters. Second, the inclusion of red-edge bands (centered at 705, 740 and 783 nm) provides high sensitivity to chlorophyll absorption and fluorescence in turbid productive waters (Mishra and Mishra 2012). Third, the shorter revisit time (5 days vs. 16 days) improves temporal sampling and reduces interpolation errors associated with ephemeral algal blooms (Drusch et al. 2012; ESA 2024). Fourth, and importantly, the current Sentinel-2 constellation (S-2A, S-2B, S-2C) enables the generation of nearly cloud-free monthly or seasonal mosaics in frequently cloud-covered regions such as temperate climate zones – a task considerably more challenging with Landsat 8/9. As demonstrated by the use of median monthly mosaics, this capability allows detection of subtle changes in chlorophyll-related signals using the four red-edge and infrared bands, which are highly sensitive to chlorophyll absorption and fluorescence (Bartold et al. 2023). This fourth advantage is particularly relevant for long-term monitoring in regions like Tehran, Iran, where seasonal cloud cover can otherwise hinder consistent time-series analysis. However, an interesting divergence emerged: although S2 achieved lower RMSE and MAE, Landsat-8 produced slightly higher $R^2$ values (e.g., 0.70 for L8-NDCI vs. 0.68 for S2-NDCI). This apparent paradox can be explained by the fact that $R^2$ measures the proportion of variance explained, which can be artificially inflated when the dynamic range of observations is limited or when errors are systematically distributed. Landsat-8's coarser resolution tends to smooth local Chl-*a* variability, producing a tighter statistical fit to the overall dataset, whereas Sentinel-2's finer-resolution captures more realistic variability, leading to lower absolute errors but slightly lower $R^2$ when the model does not perfectly follow every fine-scale fluctuation (Seegers et al. 2018). For management applications requiring accurate concentration estimates (e.g., assessing compliance with water quality thresholds), RMSE is a more relevant metric than $R^2$; therefore, Sentinel-2 is preferred for operational monitoring of Chitgar Lake.

Figure 3 illustrates the performance of L8 and S2 models in estimating Chl-*a* concentrations, with scatter plots showing the relationship between observed and estimated values for the 2BAND, NDCI and GNDVI algorithms; L8 models exhibit higher coefficients of determination ($R^2$), with the 2BAND model reaching 0.69, indicating a stronger correlation compared to S2 models, which have $R^2$ values ranging from 0.64 to 0.68, suggesting that Landsat-8 more accurately captures the variance in Chl-*a* concentrations across the study area. Figure 4 demonstrates that both the L8-NDCI and S2-NDCI models effectively predicted Chl-*a* concentrations across a wide range of values, capturing the trends in both low and high concentration levels. For the L8-NDCI Index, the observed Chl-*a* values range approximately from 0 to 10 mg/m$^3$, with the model generally following the observed fluctuations, although it tends to underestimate peak concentrations at higher values. In contrast, the Sentinel-2 NDCI Index model also covers a similar observed Chl-*a* range and shows close alignment with observed data, particularly in capturing the magnitude of higher concentrations and the variability at lower concentrations.

A comparative analysis of Chl-*a* concentrations in Chitgar Lake, derived from satellite imagery using the NDCI index (Fig. 5), highlights notable agreement with measured field data across multiple dates. As depicted in the provided maps, the Sentinel-2 and Landsat-8 platforms yield spatially consistent patterns of Chl-*a* distribution over time, with both satellites showing higher average concentrations in August 2022 and August 2023, followed by a marked decrease in August 2024. The estimated values derived from satellite-based NDCI imagery appear to closely mirror *in-situ* measurements, indicating robust performance of the remote sensing approach even amidst seasonal and interannual variations. Minor spatial discrepancies observed between the two satellites and ground-truth measurements may be attributed to differences in sensor spectral characteristics, atmospheric correction algorithms and revisit intervals. Overall, these results demonstrate the reliability and efficiency of NDCI-based satellite retrievals for monitoring temporal and spatial changes in Chl-*a* in freshwater ecosystems like Chitgar Lake, supporting

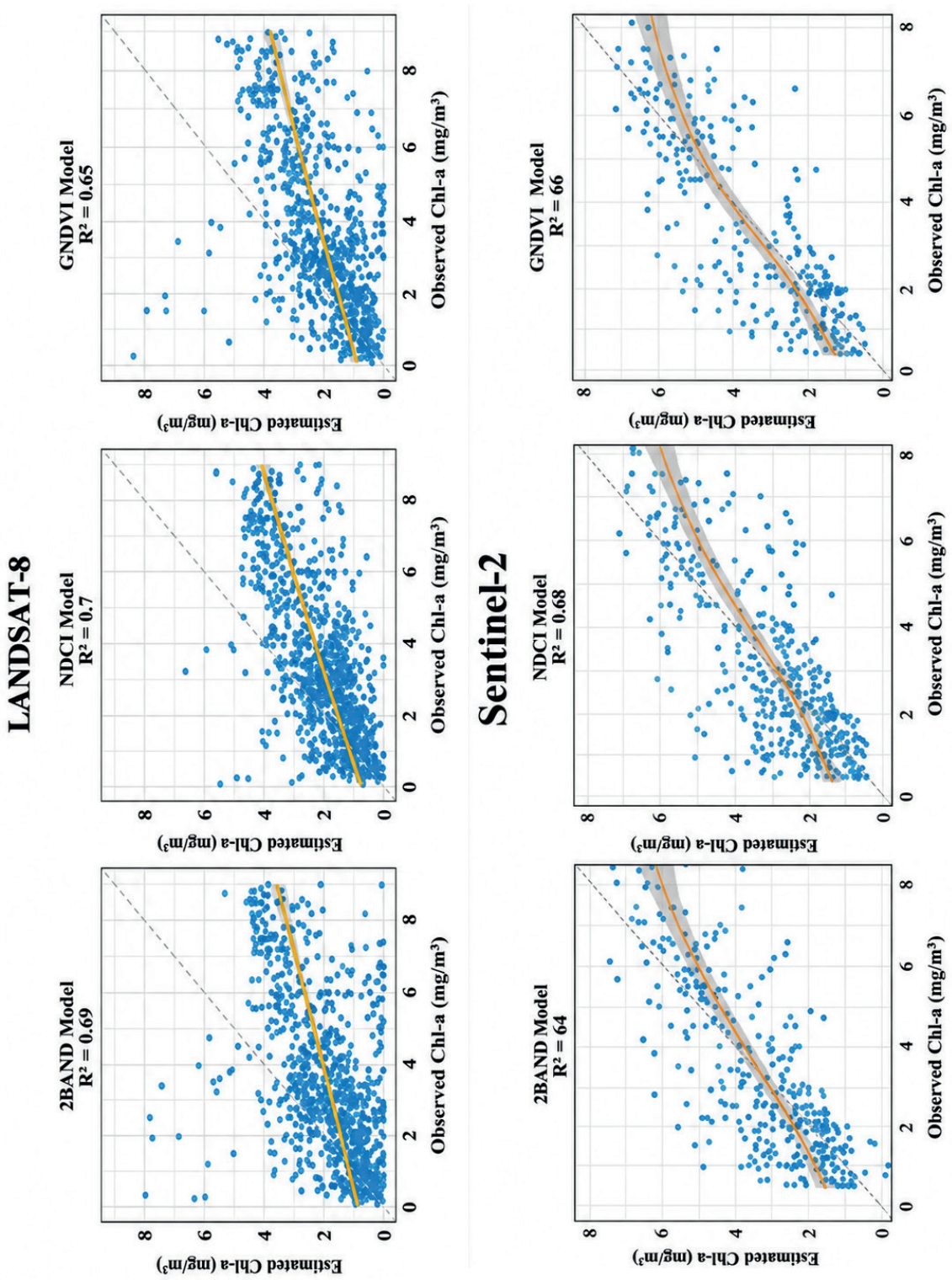


Fig. 3. Correlation between observed and predicted Chl-a concentrations derived from L8 and S2 satellite imagery

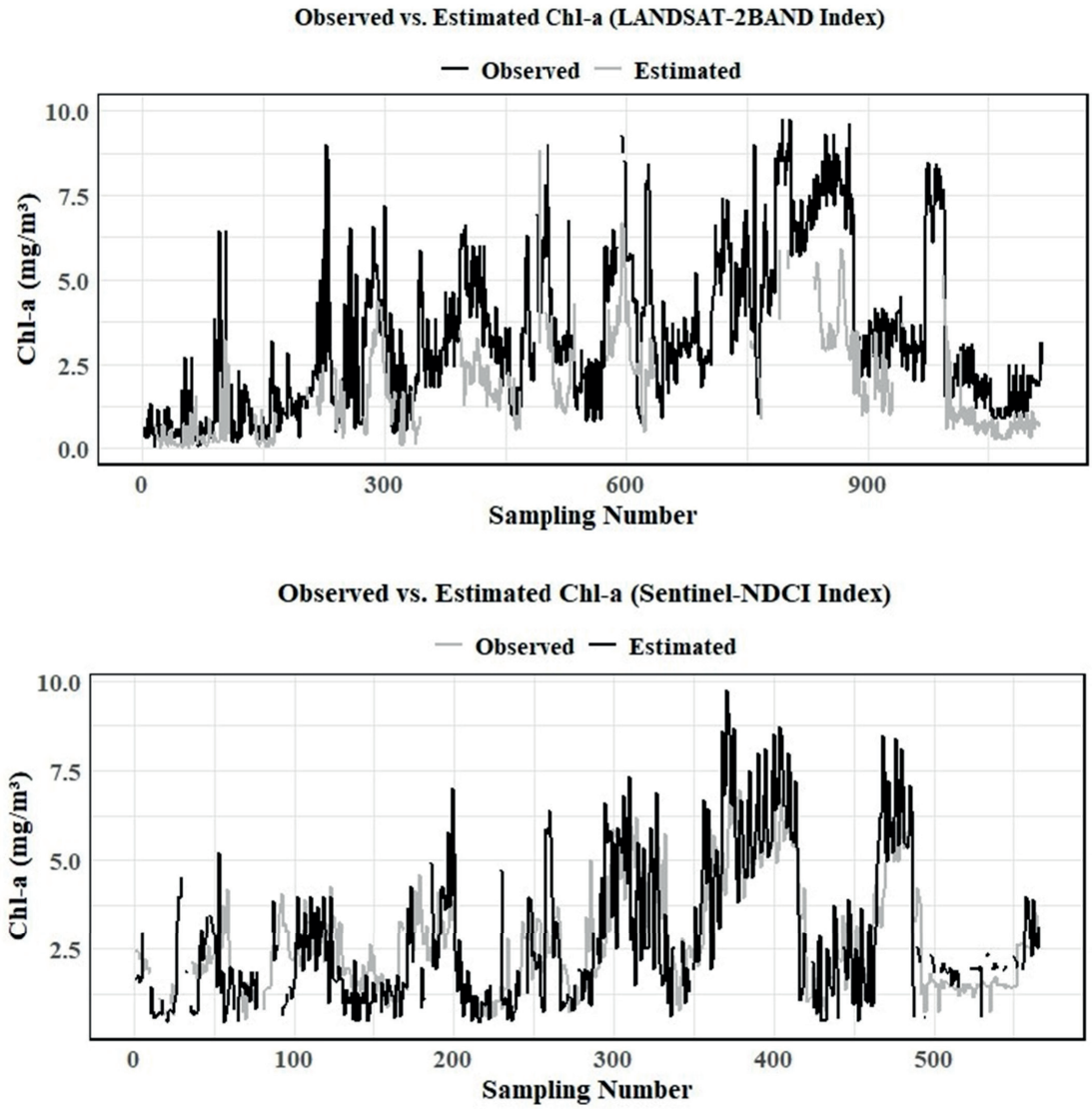


Fig. 4. Comparison of observed and estimated Chl-a concentrations, (Top: L8-2BAND Index; Bottom: S2-GNDVI Index)

their use for routine and large-scale environmental assessment. The differences in estimation accuracy between Sentinel-2 and Landsat-8 can be attributed to factors such as spatial resolution differences (S-2 generally offering finer spatial resolution), sensor spectral response variability and atmospheric correction methodologies. Sentinel-2's lower RMSE and MAE values indicate better sensitivity and capability in capturing fine-scale Chl-*a* variability in Chitgar Lake, reinforcing the robustness of its NDCI-derived estimates.

Several unavoidable uncertainties affect the present results. First, the mean Chl-*a* concentration in Chitgar Lake (3.16 mg/m$^3$) is relatively low, approaching the detection limit of both sensors, particularly for Landsat-8's 12-bit radiometric resolution. At such low concentrations, the signal-to-noise ratio (SNR) degrades, leading to higher relative errors and explaining why winter models (lowest Chl-*a*) showed poor $R^2$ despite low RMSE (Topp et al. 2020). Second, the cubic relationship observed in all algorithms (2BAND, NDCI, GNDVI) indicates non-linear optical behavior, which amplifies uncertainty at higher Chl-*a* concentrations (>8 mg/m$^3$). This non-linearity is consistent with theoretical and experimental findings in turbid productive waters (Dall'Olmo and Gitelson 2005; Gitelson et al. 2008) and implies that extrapolation beyond the calibrated range (1–10 mg/m$^3$) would be unreliable without further validation. Third, no regional tuning of atmospheric correction was applied;

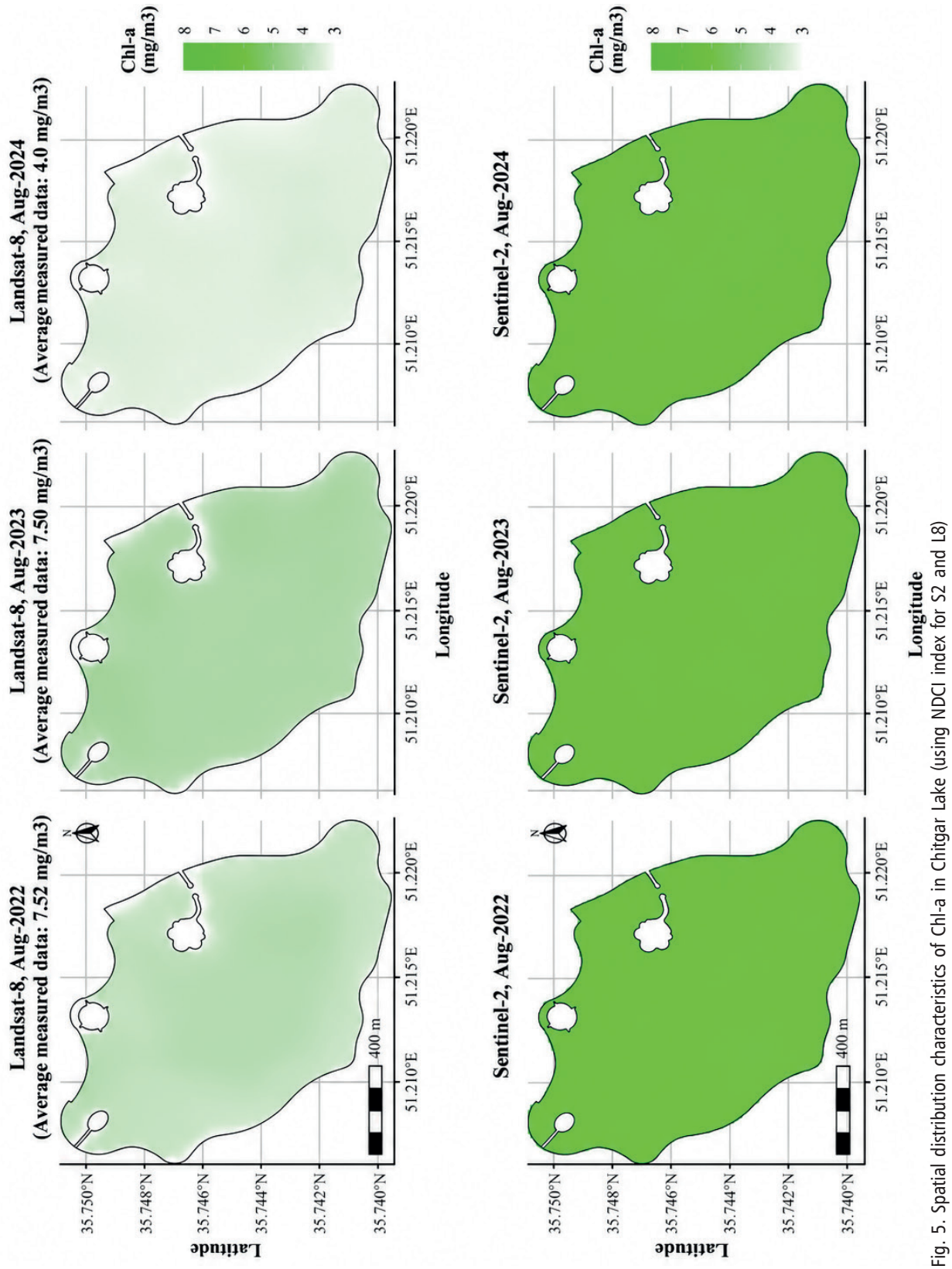


Fig. 5. Spatial distribution characteristics of Chl-a in Chitgar Lake (using NDCI index for S2 and L8)

standard algorithms (Sen2Cor, LaSRC) are optimized for ocean or clear inland waters and may introduce systematic biases in the presence of suspended sediments or colored dissolved organic matter (Frouin et al. 2019). Fourth, the statistical power of 1.00 for S2 models indicates a very low probability of Type II errors (false negatives), but Type I errors (false positives) remain possible given moderate $R^2$ values.

The approach developed here is not inherently limited to urban lakes such as Chitgar. The NDCI algorithm has been successfully applied across a range of freshwater systems, including temperate reservoirs (Beck et al. 2016), hypertrophic lakes (Ha et al. 2017), and protected areas such as El-Burullus Lake, Egypt – a RAMSAR site affected by progressive eutrophication (Assar 2024). However, two key conditions govern successful transferability: the target water body must have Chl-*a* concentrations broadly within the calibrated range (approximately 1–10 mg/m$^3$), and site-specific atmospheric correction and validation with local *in-situ* data are required, particularly for protected areas where existing monitoring may be sparse. For lakes with significantly higher TP (>0.05 mg/L) and frequent blooms, the higher RMSE of Landsat-8 could lead to underestimation of peak Chl-*a*, potentially resulting in false compliance with regulatory thresholds (Baker et al. 2021); therefore, Sentinel-2 with red-edge bands is strongly recommended for eutrophic and hypereutrophic systems. Future research should prioritize the following directions: regional atmospheric correction tuning using algorithms such as ACOLITE or POLYMER; integration of machine learning approaches (e.g., random forest or neural networks) to capture non-linear interactions between Chl-*a*, TP, temperature, and DO; comparative or combined use of Sentinel-2 and Landsat-8 data (stopping short of true pixel-level data fusion, which would require generating a unified dataset) to leverage Sentinel-2's high spatial/spectral resolution alongside Landsat-8's longer temporal archive (since 2013) for generating consistent long-term Chl-*a* time series; season-specific algorithm calibration to improve annual accuracy given the marked seasonal variability in model performance; and testing transferability to protected lakes experiencing progressive eutrophication for conservation-oriented monitoring. In conclusion, this study demonstrates that Sentinel-2 MSI, particularly the NDCI algorithm, provides more accurate and reliable Chl-*a* estimates for Chitgar Lake than Landsat-8 OLI, owing to its red-edge bands, finer spatial resolution and shorter revisit time. However, users must acknowledge remaining uncertainties related to atmospheric correction, low Chl-*a* ranges and non-linear optical responses. With appropriate calibration and validation, the proposed methodology is transferable to other urban lakes as well as protected areas affected by eutrophication, thereby supporting routine environmental monitoring and early warning of harmful algal blooms.

## Conclusion

This study investigated a comprehensive assessment of Chl-*a* concentration estimation in Chitgar Lake from 2013 to April 2025, integrating seasonal *in-situ* water quality parameter analyses with satellite-derived retrievals from S2 and L8 platforms. The observed temporal patterns in Chl-*a* correspond closely with variations in temperature, dissolved oxygen, oxygen saturation, and total phosphorus, emphasizing the ecological dynamics governing algal biomass fluctuations in the lake. Elevated Chl-*a* concentrations during summer months, particularly in August, coincide with warmer temperatures and nutrient availability, supporting characteristic eutrophic responses. The satellite-derived Chl-*a* estimates leveraging the normalized difference chlorophyll index (NDCI), two-band ratio (2BAND) and GNDVI algorithms revealed moderate to strong correlations with observed data. Sentinel-2 provided superior estimation accuracy with lower RMSE and MAE values, and moderate to good explanatory power ($R^2$: 0.64–0.68) across indices. Seasonal evaluation indicated fall as the most reliable period for Chl-*a* prediction using S2, whereas winter yielded lowest error metrics but limited explanatory power due to reduced Chl-*a* variability. L8 exhibited higher overall error but maintained strong explanatory capabilities ($R^2$ up to 0.70), with consistent seasonal performance patterns reflecting sensor-specific characteristics and resolution constraints. Spatial and temporal comparisons of Chl-*a* distributions from both satellites demonstrated consistent patterns and effectively captured interannual variations, with notable agreement to *in-situ* measurements. Differences in estimation accuracy are attributed primarily to spatial resolution disparities and atmospheric correction methodologies, with S2 offering enhanced sensitivity to fine-scale Chl-*a* variability in the lake ecosystem. Collectively, these results affirm the reliability and

efficiency of satellite-based NDCI algorithms, especially when applied to Sentinel-2 imagery, for routine monitoring of phytoplankton biomass in freshwater lakes like Chitgar. The combined use of multisensor remote sensing data alongside *in-situ* observations can substantially improve water quality assessment and management strategies, providing essential support for environmental monitoring programs. Future work should focus on refining algorithm calibration for local optical conditions and enhancing temporal coverage to capture dynamic ecological processes influencing Chl-*a* distributions.

## Data availability statement

The in-situ measurement data and satellite-derived datasets used in this study are not publicly archived but are available from the corresponding author upon reasonable request.

## Disclosure statement

No potential conflict of interest was reported by the authors.

## Author contributions

Study design: JB; data collection: JB, MRK, MK; statistical analysis: JB; manuscript preparation: JB, MRK, AS, HH; literature review: JB, MRK, AS, HH.

## References

ANSPER A and ALIKAS K, 2019, Retrieval of Chlorophyll-*a* from Sentinel-2 MSI Data for the European Union Water Framework Directive Reporting Purposes. *Remote Sensing* 11(1): 64. DOI: https://doi.org/10.3390/rs11010064.

ASSAR W, 2024, Retrieval of Chlorophyll-*a* and Vegetation Indices Using Sentinel-2 MSI Imagery in El-Burullus Lake, Egypt. *SVU-International Journal of Engineering Sciences and Applications* 5(1): 79–88. DOI: https://doi.org/10.21608/svusrc.2023.218492.1134.

AUGUSTO-SILVA PB, EVANGELISTA H, CARVALHO LM, OMETTO JP, ESPÍRITO-SANTO FG and DALL'OLMO G, 2014, Analysis of MERIS Reflectance Algorithms for Estimating Chlorophyll-*a* Concentration in a Brazilian Reservoir. *Remote Sensing* 6(12): 11689–11707. DOI: https://doi.org/10.3390/rs61211689.

BAKER DB, GARRISON PJ and WRIGHT MS, 2021, Monitoring Nutrient and Chlorophyll-*a* Levels in Lakes to Predict Algal Bloom Threats. *Water Research* 189: 116575. DOI: https://doi.org/10.1016/j.watres.2020.116575.

BALI M and GUEDDARI M, 2019, Removal of Phosphorus from Secondary Effluents Using Infiltration–Percolation Process. *Applied Water Science* 9: 54. DOI: https://doi.org/10.1007/s13201-019-0945-5.

BARTOLD M and KLUCZEK M, 2023, A Machine Learning Approach for Mapping Chlorophyll Fluorescence at Inland Wetlands. *Remote Sensing* 15(9): 2392. DOI: https://doi.org/10.3390/rs15092392.

BAYAT J, HASHEMI SH, NIKZAD MF and TALAKESH SMR, 2021, Necessity of Water Treatment to Meet Lake Water Quality Goals in Chitgar Lake. *Lake and Reservoir Management* 37(2): 160–169. DOI: https://doi.org/10.1080/10402381.2020.1843569.

BECK R, ZHAN S, LIU H, TONG S, YANG B, XU M, YE Z, HUANG Y, SHU S, WU Q, WANG S, BERLING K, MURRAY A, EMERY E, REIF M, HARWOOD J, YOUNG J, NIETCH C, MACKE D, MARTIN M, STILLINGS G, STUMPF R and SU H, 2016, Comparison of Satellite Reflectance Algorithms for Estimating Chlorophyll-*a* in a Temperate Reservoir Using Coincident Hyperspectral Aircraft Imagery and Dense Surface Observations. *Remote Sensing of Environment* 178: 15–30. DOI: https://doi.org/10.3390/rs9060538.

BREHOB MM, PENNINO MJ, HANDLER AM, COMPTON JE, LEE SS and SABO RD, 2024, Estimates of Lake Nitrogen, Phosphorus, and Chlorophyll-*a* Concentrations to Characterize Harmful Algal Bloom Risk across the United States. *Earth's Future* 12(8): e2024EF004493. DOI: https://doi.org/10.1029/2024EF004493.

CARLSON RE, 1977, A Trophic State Index for Lakes. *Limnology and Oceanography* 22(2): 361–369. DOI: https://doi.org/10.4319/lo.1977.22.2.0361.

CHEN Q, HUANG M, XIAOJUAN L and others, 2020, An Optimal Two-Band Ratio Model to Monitor Chlorophyll-*a* in Urban Lakes Using Landsat-8 Data. *E3S Web of Conferences* 20003. DOI: https://doi.org/10.1051/e3sconf/20202003003.

DALL'OLMO G and GITELSON AA, 2005, Effect of Bio-Optical Parameter Variability on the Remote Estimation of Chlorophyll-*a* Concentration in Turbid Productive Waters: Experimental Results. *Applied Optics* 44(3): 412–422.

DEMBOWSKA E, MAZUR-MARZEC H and BODZEK M, 2022, Assessing the Impact of Nutrient Loading on Phytoplankton Community Structure: A Case Study of a Eutrophic Lake. *Environmental Pollution* 300: 118841.

DRUSCH M, DEL BELLO U, CARLIER S, COLIN O, FERNÁNDEZ V, GASCON F and others, 2012, Sentinel-2: ESA's Optical High-Resolution Mission for GMES Operational Services. *Remote Sensing of Environment* 120: 25–36. DOI: https://doi.org/10.1016/j.rse.2011.11.026.

EUROPEAN SPACE AGENCY (ESA), 2024, Sentinel-2 – Instrument Payload. Copernicus Sentinel Online. Available at: https://sentinels.copernicus.eu.

FROUIN RJ, FRANZ BA, IBRAHIM A, KNOBELSPIESSE K, AHMAD Z, CAIRNS B and others, 2019, Atmospheric Correction of Satellite Ocean-Color Imagery during the PACE Era. *Frontiers in Earth Science* 7: 145. DOI: http://dx.doi.org/10.3389/feart.2019.00145.

GHOLIZADEH MH, MELESSE AM and REDDI L, 2016, A Comprehensive Review on Water Quality Parameters Estimation Using Remote Sensing Techniques. *Sensors* 16(8): 1298. DOI: https://doi.org/10.3390/s16081298.

GHOLIZADEH M, KHOSRAVI H and GHASEMI M, 2016, Remote Sensing Applications for Monitoring Chlorophyll-*a* Concentration: A Review on Algorithms and Techniques. *Journal of Environmental Management* 183: 1–12. DOI: https://doi.org/10.3390/s16081298.

GITELSON AA, DALL'OLMO G and RUNDQUIST DC, 2003, A Novel Algorithm for Remote Estimation of Chlorophyll-*a* Concentration in Turbid Waters. *IEEE Transactions on Geoscience and Remote Sensing* 41(10): 2355–2364.

GITELSON AA, DALL'OLMO G, MOSES WJ and others, 2008, A Simple Semi-Analytical Model for Remote Estimation of Chlorophyll-*a* in Turbid Waters. *Remote Sensing of Environment* 112(10): 3482–3493. DOI: https://doi.org/10.1016/j.rse.2008.04.015.

HA NTT, KOIKE K, NHUAN MT, CANH BD, THAO NTP and PARSONS M, 2017, Landsat 8/OLI Two-Band Ratio Algorithm for Chlorophyll-*a* Concentration Mapping in Hypertrophic Waters. *IEEE Journal of Selected Topics in Applied Earth Observations and Remote Sensing* 10(11): 4919–4929. DOI: DOI: https://doi.org/10.1109/JSTARS.2017.2739184.

HALLEGRAEFF GM, ANDERSON DM, BELIN C and others, 2021, Perceived Global Increase in Algal Blooms Is Attributable to Intensified Monitoring and Emerging Bloom Impacts. *Communications Earth & Environment* 2: 117. DOI: https://doi.org/10.1038/s43247-021-00178-8.

HE Y, JIN S and SHANG W, 2021, Water quality Variability and related factors along the Yangtze River using Landsat-8. *Remote Sensing* 13(12): 2241. DOI: https://doi.org/https://doi.org/10.3390/rs13122241.

KUMAR S, RANJAN P and KUMAR V, 2017, Remote Sensing Applications for Monitoring Total Suspended Solids in Coastal Waters: A Review. *Marine Pollution Bulletin* 114(2): 1150–1162.

LI C, ROUSTA I, OLAFSSON H and ZHANG H, 2023, Lake Water Quality and Dynamics Assessment during 1990–2020: A Case Study of Chao Lake, China. *Atmosphere* 14(2): 382. DOI: https://doi.org/10.3390/atmos1402038.

MISHRA S and MISHRA DR, 2012, Normalized Difference Chlorophyll Index. *Remote Sensing of Environment* 117: 394–406. DOI: https://doi.org/10.1016/j.rse.2011.10.016.

MISHRA S, STUMPF RP and MEREDITH A, 2019, Evaluation of RapidEye Data for Mapping Algal Blooms in Inland Waters. *International Journal of Remote Sensing* 40: 2811–2829. DOI: https://doi.org/10.1080/01431161.2018.1533657.

NÜRNBERG GK, 2009, Assessing Internal Phosphorus Load—Problems to Be Solved. *Lake and Reservoir Management* 25(4): 419–432. DOI: https://doi.org/10.1080/00357520903458848.

PAERL HW and PAUL VJ, 2020, Climate Change and Harmful Algal Blooms. *Harmful Algae* 91: 101731.

PARK J, KHANAL S, ZHAO K and BYUN K, 2024, Remote Sensing of Chlorophyll-*a* and Water Quality over Inland Lakes. *Remote Sensing* 16: 2761. DOI: https://doi.org/10.3390/rs16152761.

PIRASTEH S and others, 2020, Evaluation of Sentinel-2 and Landsat 8 Images for Estimating

Chlorophyll-*a* Concentrations. *Remote Sensing* 12(15): 2437. DOI: https://doi.org/https://doi.org/10.3390/rs12152437.

R CORE TEAM, 2023, R: A Language and Environment for Statistical Computing. Vienna: R Foundation for Statistical Computing.

SEEGERS BN, STUMPF RP, SCHAEFFER BA, LOFTIN KA and WERDELL PJ, 2018, Performance metrics for the assessment of satellite data products: an ocean color case study. *Optics Express* 26(6). DOI: https://doi.org/10.1364/OE.26.007404.

SHI J, SHEN Q, YAO Y and others, 2022, Estimation of Chlorophyll-*a* Concentrations in Small Water Bodies. *Remote Sensing* 14(1): 229. DOI: https://doi.org/10.3390/rs14010229.

SONARGHARE PC, MASRAM SC, SONPAROTE UR, KHAPARDE KP and KHARKATE SK, 2020, Causes and Effects of Eutrophication on Aquatic Life. *International Journal of Environmental Rehabilitation and Conservation* XI(SP2): 213–218.

TOPP SN, PAVELSKY TM, JENSEN D, SIMARD M and ROSS MRV, 2020, Research Trends in the Use of Remote Sensing for Inland Water Quality Science. *Water* 12(1): 169. DOI: https://doi.org/10.3390/w12010169.

U.S. GEOLOGICAL SURVEY, 2023, Landsat 8–9 Data Users Handbook. U.S. Geological Survey.

VERZANI J, 2004, Using R for Introductory Statistics (Second Edition). Chapman and Hall/CRC. DOI: https://doi.org/https://doi.org/https://doi.org/10.4324/9780203499894.

ZHANG S, QIU B and WANG H, 2023, Nutrient Management Strategies to Mitigate Harmful Algal Blooms. *Journal of Environmental Management* 316: 115228.

ZHANG Y, WANG Y and ZHANG S, 2018, Estimation of Chlorophyll-*a* Concentration in Lakes Using Landsat Imagery. *Remote Sensing Letters* 9(5): 482–491. DOI: https://doi.org/10.1007/s11356-020-07706-7.

*Received 19 February 2026*
*Accepted 8 June 2026*